

L-Vertical-shaped 3D Silicon Modulator for Efficient High-speed Communication

1st Zijian Zhu

National Key Laboratory of Materials for Integrated Circuits, Shanghai Institute of Microsystem and Information Technology, Chinese Academy of Sciences University of Chinese Academy of Sciences Shanghai, China zhuzj@mail.sim.ac.cn

2nd Yingxuan Zhao

National Key Laboratory of Materials for Integrated Circuits, Shanghai Institute of Microsystem and Information Technology, Chinese Academy of Sciences Shanghai, China zhaoyx@mail.sim.ac.cn

3rd Fuwan Gan

National Key Laboratory of Materials for Integrated Circuits, Shanghai Institute of Microsystem and Information Technology, Chinese Academy of Sciences Shanghai, China fuwan@mail.sim.ac.cn

Abstract—Doping profiles in the rib waveguide have been significant in silicon modulator design. As doping regulation in the cross-section reaches limitation, complex optimization in three dimensions has great potential to improve performance remarkably. This work proposes a modulator based on L-shaped and vertical junctions for high-speed communication. The results show that at -1 V bias, the modulation efficiency of the design is 0.81 V·cm, while the loss is 14.3 dB/cm, and the bandwidth is over 45 GHz. This modulator is applicable for high-baud optical links and illustrates the great potential of 3D modulator design.

Keywords—silicon modulator, 3D design, modulation efficiency, bandwidth, high-speed communication

I. INTRODUCTION

Silicon photonics (SiP) has emerged as a promising solution for short-reach to long-haul optical links, due to its complementary metal-oxide semiconductor (CMOS) compatibility and fine optical confinement. The silicon platform enables compact footprints of waveguides and thus large-scale integration. Among all the components of an optical transmission link, the electro-optic modulator plays a significant role to transmit high-baud data. Mach-Zehnder modulators (MZMs) and microring modulators (MRMs) based on the plasma dispersion effect are mainly applied in SiP. MZMs are commonly adopted in commercial optical transmitters for better thermal insensitivity and large fabrication tolerance compared with MRMs. To modulate light through the plasma dispersion effect, the charge density within the optical waveguide is manipulated by driving voltages. MZMs based on carrier depletion present benefits of high operation speed and low power consumption, thus mostly studied. Therefore the p-n junction generated by the doping profile is crucial. The optimization of doping profiles implemented in the rib waveguide cross-section produces various junction types of silicon modulators such as the lateral junction, the vertical junction, the L-shaped junction and the wrapped junction [1]. However, the adjusting

of doping profiles in the rib cross-section is limited by the waveguide size. As junctions in the light propagation direction are also proved effective to improve modulation efficiency and reduce propagation loss [2] [3], the appropriate composition of doping profiles that generate p-n junctions both in the cross-section and in the propagation direction, namely 3D optimization, has great potential to strongly enhance the modulator performance. For the purpose of improving the typical figure of merit (FOM) as $V_\pi \alpha L$ [4] [5] to a certain low value and obtaining broad electro-optic (EO) bandwidth, we propose the modulator comprised of the L-shaped junction and the vertical junction. Both kinds of junctions focus on decreasing $V_\pi L$. The combination of these two types of junctions in this work, namely the L-Vertical-shaped modulator, demonstrates a 3D design with the $V_\pi L$ of 0.81 V·cm and high bandwidth of 45 GHz, proving the effectiveness and potential of 3D modulator design.

II. METHODS

To generate accurate 3D p-n junctions, the doping profiles are simulated by the 3D Monte-Carlo method [6]. The structure of 3D modulator in this work is demonstrated in Fig.1. Fig.1(a) is the top view of the MZM whose modulating arm consists of multiple periods. The region between the black dashed lines is one period, which is denoted by Fig.1(b). Each period has two parts, named the former part and the latter part, respectively. The doping for the former part has an active region length of L_{p1} and the latter doping region length is L_{p2} . In this work we have $L_{p1}=L_{p2}$. The cross-section of the 3D MZM is shown in Fig.1(c), based on the typical 220-nm SOI wafer whose buried oxide (BOX) is 2 μm . The width of the rib waveguide is 410 nm and the height of the slab is 60 nm to meet the single-mode condition. To achieve excellent performance as decreasing $V_\pi \alpha L$ and broadening EO bandwidth, we optimize the doping doses, doping energies and doping locations in the X direction for both former and latter doping. The optimization is within the limits of the ordinary two-step manufacturing process, thus the results are applicable

regarding practical requirements. 3D electrical simulation is performed at biases to obtain varying doping profiles, resulting in modulation efficiency ($V_{\pi}L$) and loss per cross-section. The $V_{\pi}L$ for this period is calculated as

$$V_{\pi}L_{total} = V_{pp} \frac{L_{tot}\lambda}{2L_z \text{sum}(\Delta n(z))} \quad (1)$$

where $\Delta n(z)$ is the effective index variation of each cross-section, λ is the wavelength, L_z is the interval between two cross-sections which is set equal, and L_{tot} is the whole length of the period.

Equivalent loss for this period is:

$$\text{Loss}_{total} = \text{sum}(\text{Loss}(z)) \frac{L_z}{L_{tot}} \quad (2)$$

where $\text{Loss}(z)$ is the loss of each cross-section.

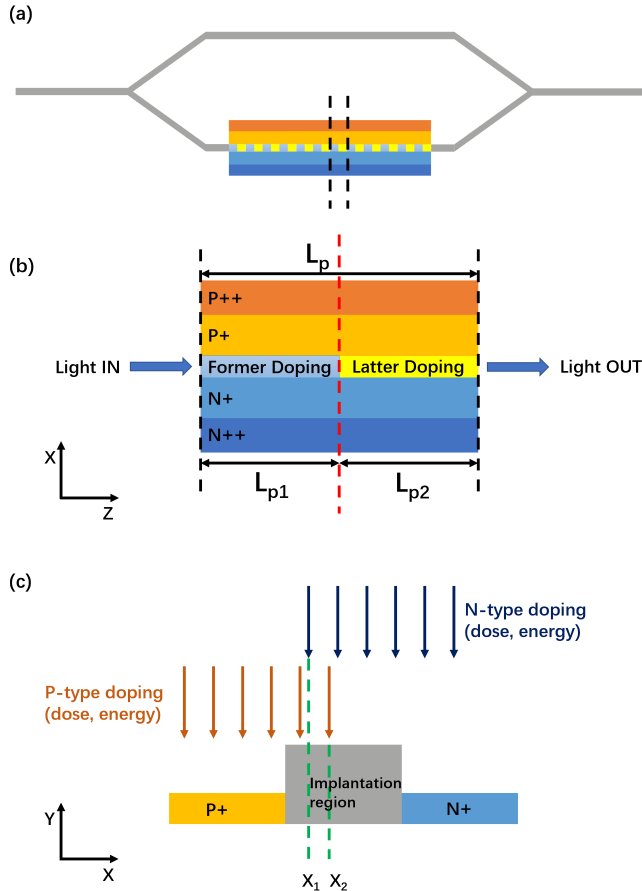


Fig. 1. (a) The top view of the 3D MZM, (b) the interdigitated period whose length is L_p has two parts (L_{p1} is the former part length, L_{p2} is the latter part length), (c) the cross-section of the modulator with two-step doping process, X_1 and X_2 are the doping locations in the X direction of N-type and P-type doping, respectively.

III. DISCUSSION

The optimized doping profile of each half of the period is depicted in Fig.2. The former doping forms the L-shaped junction and the latter doping forms the vertical junction. The

doping level is around $1e18$ to balance the efficiency, loss and impedance.

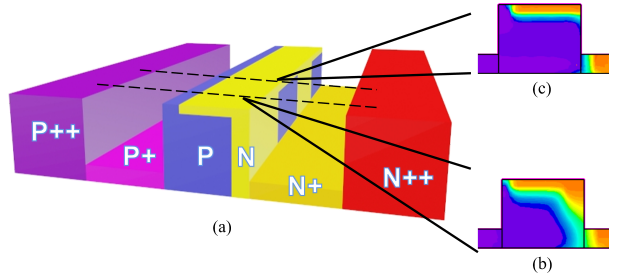


Fig. 2. (a) Schematic diagram of the designed modulator based on L-shaped and vertical junctions; (b) the former half is the L-shaped junction and (c) the latter half is the vertical junction.

The simulation results of equivalent $V_{\pi}L$, carrier-induced loss, resistance and capacitance of the designed modulator are shown in the following. By V_{pp} being 2V, the overall $V_{\pi}L$ of the period at the bias of -1 V is 0.81 V·cm and the insertion loss is 14.3 dB/cm, as denoted by Fig.3 and Fig.4. Fig.3 demonstrates the reason for high modulation efficiency as the interface between two parts of the period drags down the $V_{\pi}L$. The junction generated at the interface in the propagation direction contributes to the $V_{\pi}L$ decrease. In addition, the latter part doping has the vertical junction above the rib center which approximately is also the center of the single mode, and the former part doping has the L-shaped junction around the mode center as well. The position of the junction enables more efficient overlap with the mode center while biased. This composition of doping profiles has depletion region expanded towards and across the mode center in three dimensions.

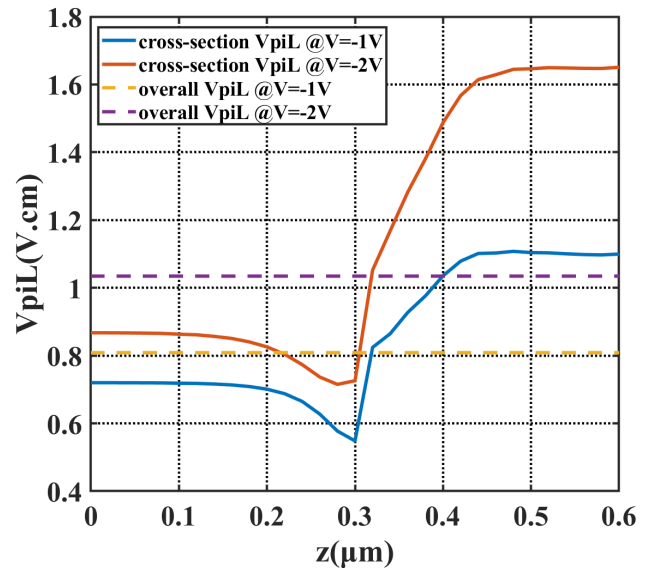


Fig. 3. $V_{\pi}L$ of the designed modulator along the propagation direction(z) under reverse biases (solid lines are the performance of each cross-section; dashed lines are the equivalent performance of the whole period).

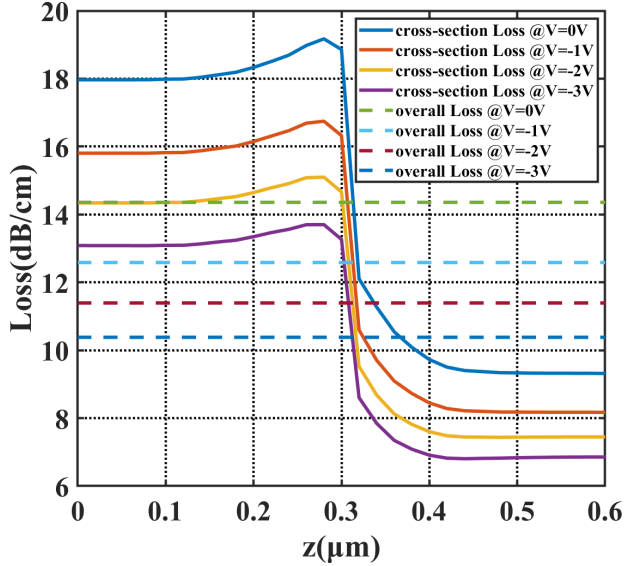


Fig. 4. Carrier-induced loss of the designed modulator along the propagation direction(z) under reverse biases (solid lines are the performance of each cross-section; dashed lines are the equivalent performance of the whole period).

The resistance and the capacitance of this period are displayed in Fig.5 and Fig.6. The resistance is ultra-high while the structure is not biased, for the electron current path is blocked both in the former and latter parts. When a high reverse bias voltage is applied, the electrons from the slab in the former part are transferred and replenished into the current channel, thus the current path is well provided by the former half. Hence the latter half is optimized specifically for modulation efficiency improvement and loss reduction. Moreover, the junction in the propagation direction at the interface of the L-shaped and vertical doping profiles is optimized to be slimmer than the interleaved PN junctions to avoid high capacitance. As a result, the capacitance is below 0.28 fF/ μ m, owing to the small-area p-n junction, yet enough to modulate light efficiently.

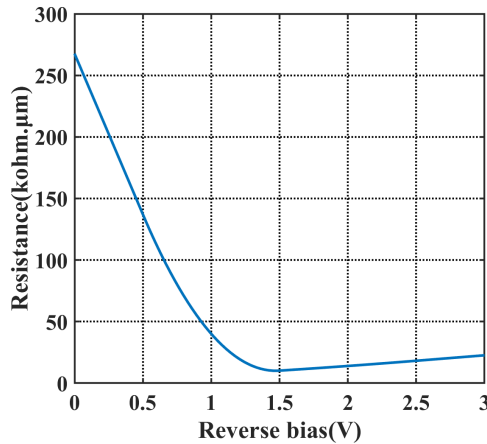


Fig. 5. Equivalent resistance of the modulator under reverse biases.

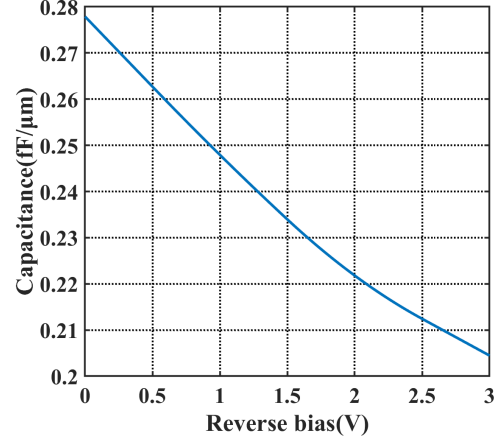


Fig. 6. Equivalent capacitance of the modulator under reverse biases.

Loaded by the transmission line satisfying the standard fab process, the EO bandwidth at -1 V bias is calculated. With the low $V_{\pi}L$ at -1 V, the active region is set to 1 mm. The normalized bandwidth is shown in Fig.7 to be over 45 GHz. The high-frequency performance caters to the requirement of high-speed optical links. Furthermore, low voltage enables low power consumption in transmission which also meets the developing trend.

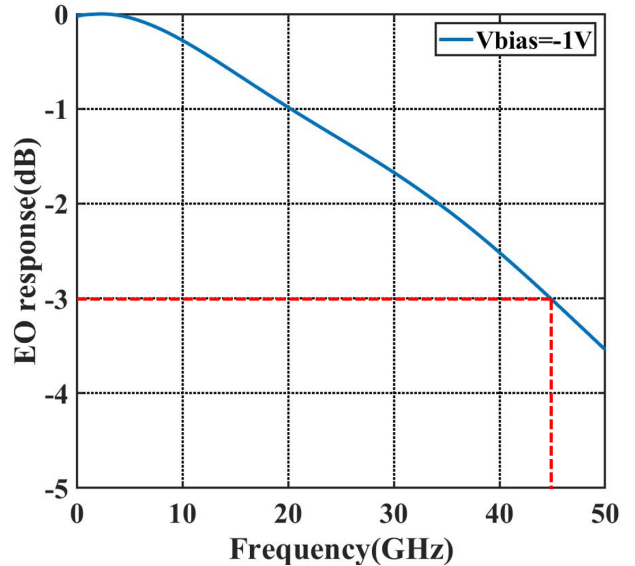


Fig. 7. The normalized frequency response at -1 V bias.

IV. CONCLUSION

To sum up, a novel modulator based on L-shaped and vertical junctions is proposed. The $V_{\pi}L$ of this structure is 0.81 V·cm while its loss is 14.3 dB/cm. The bandwidth extends over 45 GHz. This design caters to the requirement of high-speed optical modules. Moreover, all the results are obtained at

-1 V bias, showing great potential for low power-consumption application.

ACKNOWLEDGMENT

The authors thank the funding provided by National key R & D Program of China (2022YFB2803100); National major scientific research instrument development project (22127901); Shanghai Sailing Program (22YF1456700).

REFERENCES

- [1] A. Rahim, A. Hermans, B. Wohlfel, D. Petousi, B. Kuyken, D. Thourhout, and R. Baets, "Taking silicon photonics modulators to a higher performance level: state-of-the-art and a review of new technologies," *Adv. Photon.*, vol. 3, pp. 024003–024003, April 2021.
- [2] M. Ziebell, D. Marris-Morini, G. Rasigade, P. Crozat, J.-M. Fédéli, P. Grosse, E. Cassan, and L. Vivien, "10 Gbit/s silicon modulator based on interdigitated PN junctions," *8th IEEE International Conference on Group IV Photonics*, London, UK, pp. 17-19, 2011.
- [3] J. C. Rosenberg, W. M. J. Green, S. Assefa, D. M. Gill, T. Barwicz, M. Yang, S. M. Shank, and Y. A. Vlasov, "A 25 Gbps silicon microring modulator based on an interleaved junction," *Opt. Express*, vol. 20, pp. 26411-26423, 2012.
- [4] X. Tu, T. Liow, J. Song, M. Yu, and G. Lo, "Fabrication of low loss and high speed silicon optical modulator using doping compensation method," *Opt. Express*, vol. 19, pp. 18029–18035, 2011.
- [5] I. Goykhman, B. Desiatov, S. Ben-Ezra, J. Shappir, and U. Levy, "Optimization of efficiency-loss figure of merit in carrier-depletion silicon Mach-Zehnder optical modulator," *Opt. Express*, vol. 21, pp. 19518–19529, 2013.
- [6] Z. Zhu, Y. Zhao, H. Huang, Y. Li, X. She, J. Zhu, H. Liao, X. Liu, R. Huang, H. Liu, Z. Sheng, and F. Gan, "Silicon modulator based on omni junctions by effective 3D Monte-Carlo method," *Opt. Express*, vol. 30, pp. 47326-47337, 2022.